Frontal instabilities within tropical instability vortices at sub-mesoscales

PSP 03 8296

L. R. Benjamin (lrb@hawaii.edu) and P. Flament (pflament@hawaii.edu)
Department of Oceanography, University of Hawaii, Marine Science Building, 1000 Pope Road, Honolulu, HI 96822

I. Introduction

Synthetic aperture radar image of surface roughness [Figure 1a] shows leading front of tropical instability vortex (TIV) [Figure 1b].

TIVs are ~500-km diameter anticyclones on North Equatorial Front subject to centrifugal instability that swirl equatorial and tropical waters, translating westward at 0.2 to 0.5 m/s [*Kennan and Flament*, 2000].

Sub-mesoscale fronts (SMFs) with 1 to 10-km length scales [Figure 2] have down-front thermal wind currents and secondary ageostrophic circulation that overturns across the front [*McWilliams*, 2016].

SMFs can be unstable, as is the front in Figure 1a with cusps and waves at 2–8 km scales.

What can we determine about the instability mechanisms involved in SMFs in TIVs?

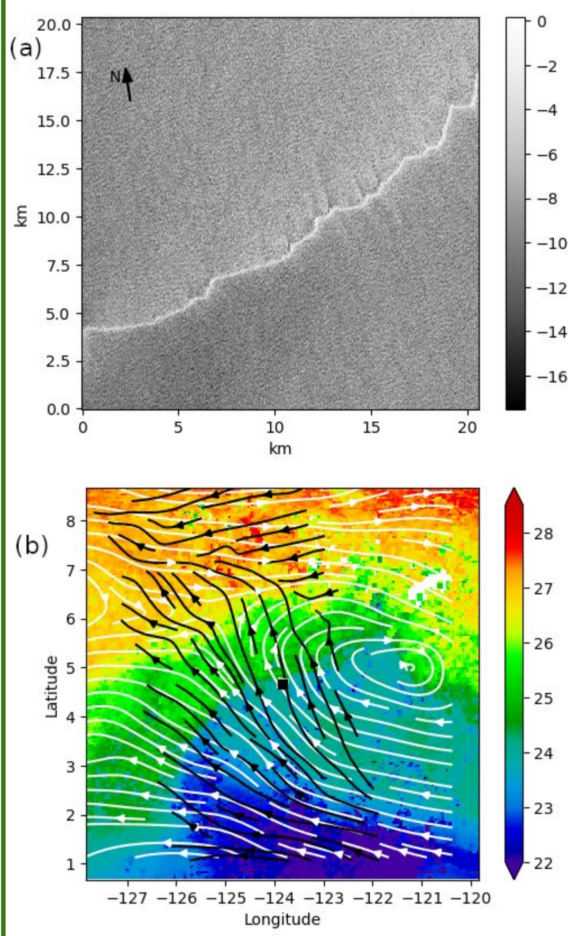

Figure 1. (a) Sentinel-1 synthetic aperture radar (SAR) image of back-scatter (dB) from 3 Jan 2018 centered at ~4.5°N, 123.5°W, with north indicated (arrow); (b) sea surface temperature (color) composite from Modis Aqua and Terra over 2-4 Jan 2018, with satellite winds (black streamlines) and SSH/model derived surface currents (white streamlines), both on 3 Jan 2018. Winds at SAR location (black square in (b)) are 5.3 m/s at 339°; currents are 0.43 m/s at 327°.

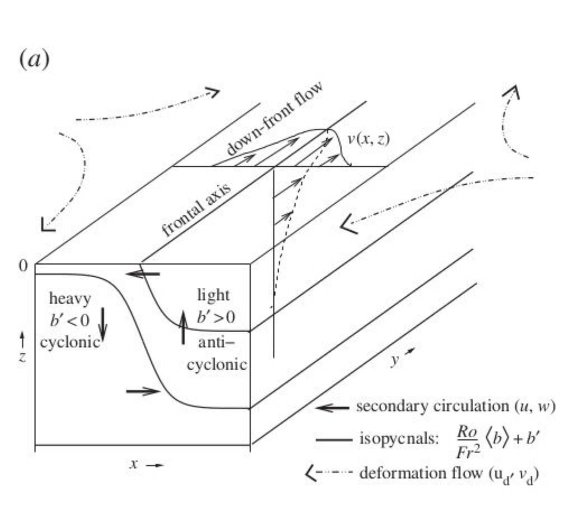

Figure 2. Diagram of sub-mesoscale front showing large-scale deformation flow (dot-dashed arrows), down-front geostrophic/thermal wind flow (solid arrows in y-direction), ageostrophic secondary circulation (solid arrows in x-z plane). From *McWilliams* [2016; Figure 5a].

II. Instabilities

Instabilities can be categorized by energy source and also potential vorticity:

$$q = \vec{\omega} \cdot \nabla b = (f+\zeta)N^2 + \vec{\omega}_h \cdot \nabla_h b = q_v + q_h$$

for PV q, vorticity $\vec{\omega}$, buoyancy b, Coriolis frequency f, vertical vorticity ζ, buoyancy frequency N, horizontal vorticity $\vec{\omega}_h$, horizontal gradient ∇_h, vertical PV q_v, and horizontal or baroclinic PV q_h.

Gravitational instability [Figure 3a]: energy from buoyancy flux
- If dense surface layer overlies stable stratification, vertical parcel perturbations can be unstable: $q_h = 0$ and $N^2 < 0$ so $q < 0$

Inertial instability [Figure 3b]: energy from shear of geostrophic current
- If geostrophic current is in stable stratification, down-SSH-gradient perturbations can be unstable: $q_h = 0$ and $\zeta < -f$ so $q < 0$

Symmetric instability [Figure 3c]: energy from thermal wind shear
- If baroclinic layer in thermal wind balance has no changes along current axis, lateral parcel perturbation can be unstable: $\vec{\omega}_h \cdot \nabla_h b = -1/f\,|\nabla_h b|^2$ so $q < 0$

Barotropic instability [Figure 3d]: energy from mean kinetic energy of jet
- If barotropic ocean has surface current, perturbation into the shear of the jet can be unstable: velocity of jet gives sign change in q_v

Baroclinic instability [Figure 3e]: energy from mean potential energy
- If baroclinic surface layer in thermal wind balance has changes along current axis , lateral parcel perturbation can be unstable, profile of jet gives sign change in q_v (not strictly necessary depending on vertical shear)

Kelvin-Helmholtz instability [Figure 3f]: energy from mean kinetic energy of shear current
- two layer system with density and shear velocity jump across interface is unstable to interface perturbations

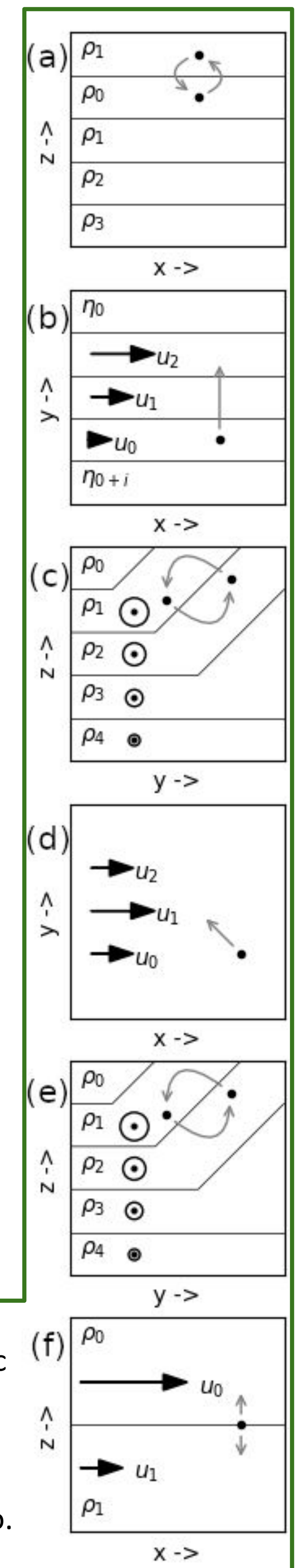

Figure 3. Simple conditions under which different instabilities may occur: (a) gravitational instability; (b) inertial instability; (c) symmetric instability; (d) barotropic instability; (e) baroclinic instability; and (e) Kelvin-Helmholtz instability. Thin lines in (a), (c), (e), and (f) are isopycnal, while those in (b) are for sea surface height. Black arrows in (b), (d), and (f) are zonal velocity, as are the vectors out of the page in (c) and (e). Grey arrows show the type of perturbation that the conditions is unstable to. In (c), there is no change in the x-direction, which is allowed in (e).

III. Results

There are two frontal regions in TIVs:

1. Leading frontal region on western flank of TIV with tropical water to west and equatorial water to east, crossed in TIWE-1 cruise [Figure 4]:
- Below light wedge Richardson numbers lower and vertical shear enhanced
- In light wedge currents are weaker and head WSW right at front
- In denser water currents are stronger and head N

2. Trailing frontal region to the east with equatorial water to west and tropical water to east, crossed in TIWE-2 cruise [Figure 5]:
- Below light wedge Richardson numbers lower and vertical shear enhanced
- Current magnitudes in light wedge are stronger than elsewhere, especially right at front near surface
- Currents rotate from WSW/W in light wedge to N below

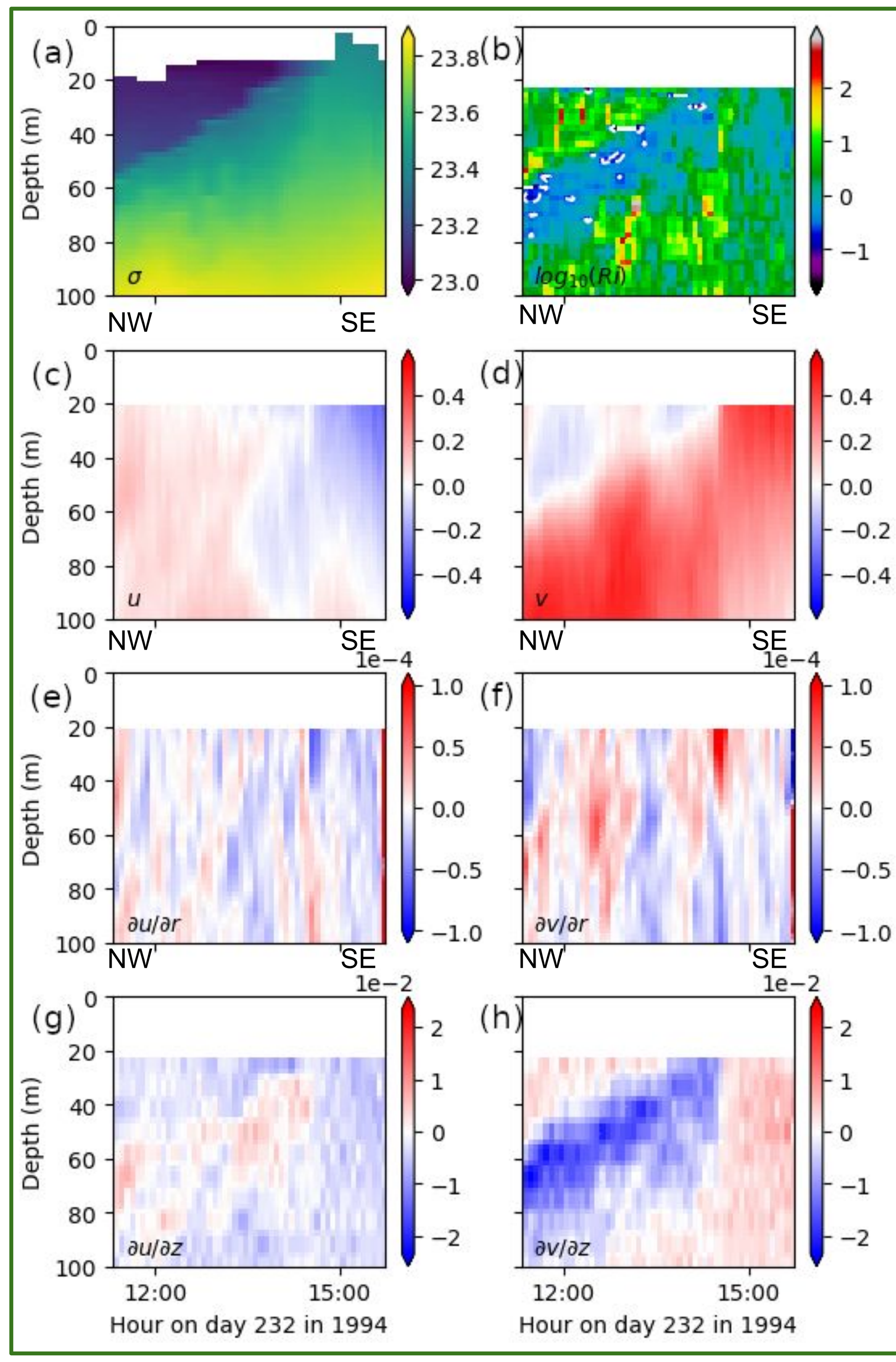

Figure 4. (a) potential density in kg/m^3; (b) log10 of Richardson number *Ri*, where areas *Ri* < 1/4 are outlined in white; (c) *u* in *m/s*; (d) *v* in m/s (e) along-track shear of *u*; (f) along-track shear of *v*; (g) vertical shear of *u*; and (h) vertical shear of *v* for TIWE-1 cruise crossing of leading front northwest to southeast at ~3.4°N, 128.8°W on 20 Aug 1994 [ADCP: *Firing et al., 1994*; CTD: *Sawyer et al.*, 1994]. The Coriolis frequency here is 4.3 x 10^{-6} s^{-1}.

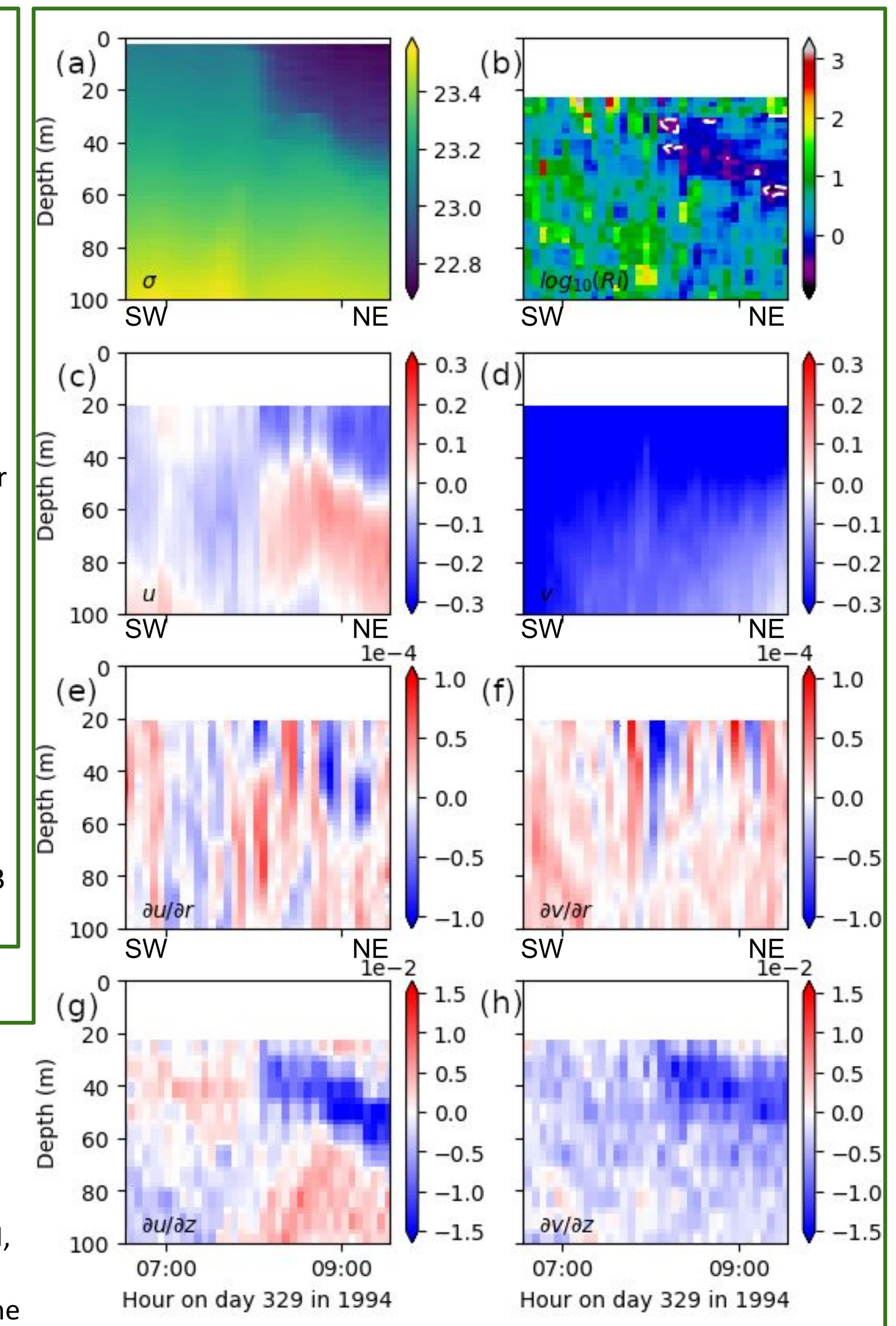

Figure 5. Same as Figure 4 but for TIWE-2 cruise crossing of trailing front, southwest to northeast at ~2.7°N, 143.2°W on 25 November 1994. The Coriolis frequency here is 3.6 x 10^{-6} s^{-1}.

Vertical shear is strong - order 3000*f*
- Relevant for baroclinic instability, Kelvin-Helmholtz instability

Horizontal shear is strong - order 40*f*
- Relevant for barotropic instability, inertial instability

Along-track buoyancy gradient is strong - order 10^{-7}
- Relevant for symmetric instability

Vertical buoyancy gradient is strong - order 10^{-4}
- Relevant for gravitational instability, Kelvin-Helmholtz instability

Richardson numbers are low - 0.2 to 0.8
- Relevant for Kelvin-Helmholtz instability

HOWEVER: cannot look at energy conversion in the TIVs - only a single transect and no timeseries, but can look to model output for PV [Figure 6, *Holmes et al.* 2014].

Vertical PV [Figure 6a]:
- Strongly positive at both leading and trailing fronts - no gravitational instability or inertial instability
- Less strong just off the fronts, i.e., fronts are maxima - could be baroclinic or barotropic instability

Horizontal PV [Figure 6b]:
- Strongly negative at both leading and trailing fronts - could be symmetric instability

Total PV [Figure 6d]:
- Strong vertical PV overcompensates for negative horizontal PV
- Positive at both leading and trailing fronts - no gravitational, inertial, or symmetric instability

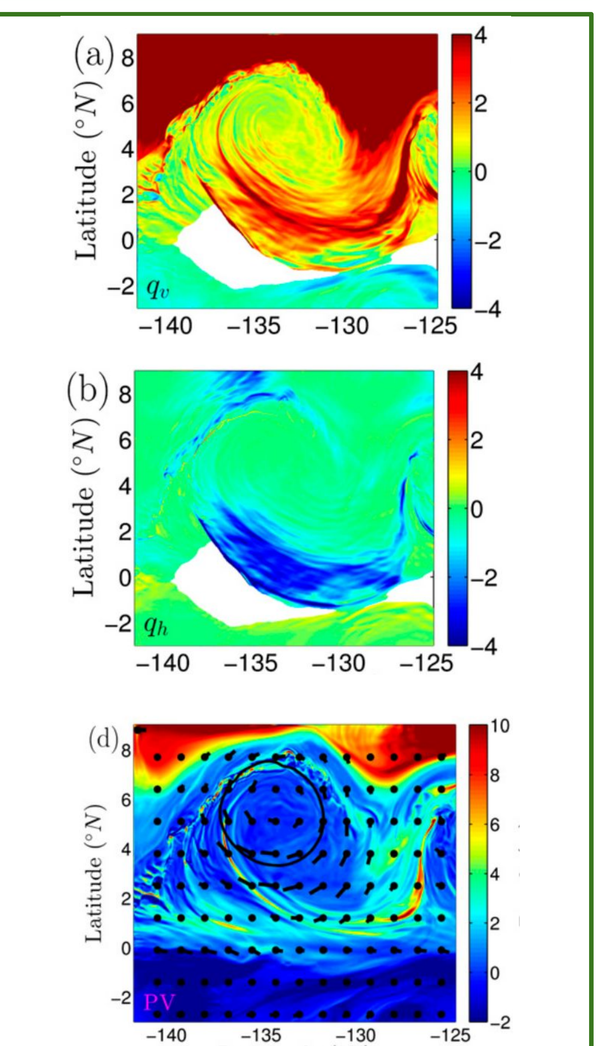

Figure 6. (a) Vertical PV and (b) horizontal PV (x 10^{-9} s^{-1}) modeled in Holmes et al. [2014; their Figure 3a and 3b]; (d) total PV (x 10^{-9} s^{-1}) modeled in *Holmes et al.* [2014; their Figure 2d].

IV. Conclusions

The leading and trailing fronts are unlikely to be subject to gravitational, inertial, or symmetric instability as total PV > 0.

These two fronts have a change in sign of vertical PV, which may indicate barotropic or baroclinic instability.

Strong horizontal shear is present at the frontal edge, and there is very strong coherent vertical shear below the wedge of less-dense water.

The leading front data shows that it may have Richardson numbers < ¼ that would allow Kelvin-Helmholtz instability, but the model does not agree. Both data and model indicate Kelvin-Helmholtz instability may occur at the trailing front.

Even more dramatic instabilities can occur on both leading and trailing fronts [Figure 7], but model studies are needed to do an analysis of the energy of the instabilities in TIV SMFs.

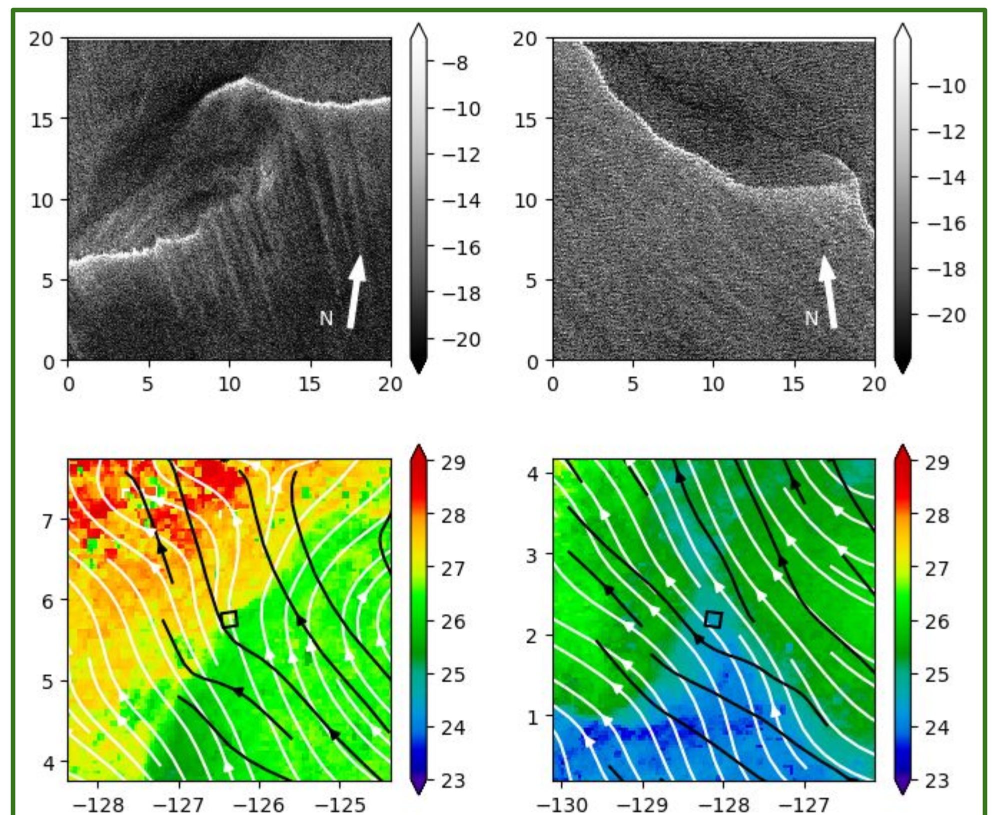

Figure 7. Same as Figure 1 but for (left column) SAR image on 5 Aug 2016 on leading front at ~6°N, 126°W; and (right column) SAR image on 30 Sep 2019 on trailing front at ~2°N, 128°W.

Acknowledgements

This study has been conducted using E.U. Copernicus Marine Service Information (https://doi.org/10.48670/moi-00050, https://doi.org/10.48670/moi-00182) for current and wind data; Copernicus Sentinel Data [2020]; and NASA Ocean Biology Processing Group information (https://doi.org/10.5067/MODSA-1D4D9, https://doi.org/10.5067/MODST-1D4D9) for sea surface temperature data.

References

Firing, J., E. Firing, P. Flament, and R. Knox, 1994: Acoustic Doppler current profiler data from R/V Moana Wave cruises MW9010 and MW9012. Tech. Rep. 93-05, SOEST, University of Hawaii, Manoa, 114 pp. [Available from Satellite Oceanography Laboratory, SOEST, University of Hawai'i at Manoa, Honolulu, HI 96822.]

Holmes, R. M., L. N. Thomas, L. Thompson, and D. Darr, 2014: Potential vorticity dynamics of tropical instability vortices. *J. Phys. Oceanogr.*, **44**, 995–1011.

Kennan, S. K., and P. J. Flament, 2000: Observations of a tropical instability vortex. *J. Phys. Oceanogr.*, **30**, 2277–2301.

McWilliams, J. C., 2016: Submesoscale currents in the ocean. *Proc. R. Soc. A.*, **472**, 20160117.

Sawyer, M., P. Flament, and R. Knox, 1994: Hydrographic SeaSoar data from the R/V Moana Wave cruises MW9010 and MW9012. Tech. Rep. 94-04, SOEST, University of Hawaii at Manoa, 101 pp. [Available from Satellite Oceanography Laboratory, SOEST, University of Hawaii at Manoa, Honolulu, HI 96822.]